

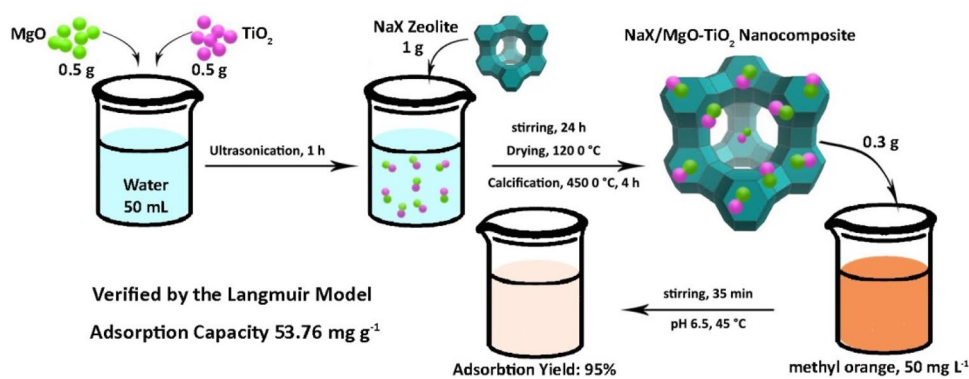


Efficacy of Novel NaX/MgO–TiO₂ Zeolite Nanocomposite for the Adsorption of Methyl Orange (MO) Dye: Isotherm, Kinetic and Thermodynamic Studies

Daryoush Mirzaei¹ · Abedin Zabardasti¹ · Yaghoob Mansourpanah¹ · Meysam Sadeghi¹ · Saeed Farhadi¹

Received: 27 August 2019 / Accepted: 25 October 2019 / Published online: 31 October 2019
© Springer Science+Business Media, LLC, part of Springer Nature 2019

Graphic Abstract



Keywords NaX/MgO–TiO₂ · Nanocomposite · Ultrasound-assisted dispersion · Adsorption · Methyl orange dye

1 Introduction

Nowadays, the growing synthetic organic dyes used in textile, leather, medical, paper, and food industries cause serious threat to human health and ecological systems because of their non-biodegradability and high toxicity [1]. Among these types of dyes, methyl orange (MO) has been recognized as one of the most well-known anionic organic dyes belonging to the class of azo dye which has an (N=N) group within its molecular structure [2]. The existence of this group over the MO dye can be very harmful and causes various disorders for the human body and environment. Accordingly, the removal of these pollutants from industrial effluents is an important issue [3]. Currently, a great deal of attention is paid to water pollution control, especially for the removal of these types of organic pollutants [4]. So far, several strategies

and methodologies such as membrane separation [5], catalytic oxidation [6], sonochemical degradation [7], adsorption process [8], have been designed and developed for removing and treating of organic dyes from wastewater. Among these methods, adsorption technology has been widely applied due to its high efficiency, flexible and simple method compared to other techniques for the removal of pollutants from effluents [9]. Organic pollutants could be removed by several types of solid materials including activated carbons [10], zeolites [11], silica gel [12], and alumina [13]. To enhance the adsorption capacity and efficiency, nanomaterials (NMs) are used as adsorbents for the removal of organic dyes from water and effluents. Indeed, owing to their high surface area and specific affinity, metal oxide nanoparticles have been able to remove the pollutants from effluents with a high capacity and faster rates [14]. Accordingly, metal oxide nanoparticles, e.g. MnO₂, Fe₃O₄, TiO₂, MgO, CdO, and ZnO have been utilized as suitable adsorbents to remove dyes and heavy metals. Among these metal oxides employed, titanium dioxide nanoparticles (TiO₂ NPs) as a n-type semiconductor with a band gap energy

✉ Abedin Zabardasti
zabardasti@yahoo.com; zabardasti.a@lu.ac.ir

¹ Department of Chemistry, Lorestan University,
68137-17133 Khorramabad, Iran

of 3.0–3.2 eV, is the most preferable adsorbent given its non-toxicity, insolubility, stability, high photoactivity, and inexpensive nature. There are three kinds of crystallographic phases for TiO_2 metal oxide including brookite, rutile, and anatase at ambient temperature [15, 16]. Among them, the anatase phase has a higher photocatalytic performance to remove the organic dyes pollutants in comparison with that of brookite and rutile phases [17]. Additionally, magnesium oxide nanoparticles (MgO NPs) with a band gap energy of 4.2 eV [18], are very effective adsorbents for the removal of these pollutions thanks to their high adsorption capacity, simplicity of their preparation, and high surface reactivity [19]. On the other hand, zeolites are recognized as crystalline hydrated aluminosilicates of group IA and IIA elements. Meanwhile, NaX zeolite (also called 13X) belongs to the family of Faujasite (FAU) which is well-known to have a higher elemental aluminum content within its crystalline framework compared to other zeolites such as NaY and ZSM-5. The linkage of β -cages or sodalite to D6R (double-6-member ring) builds its structure leading to the formation of a large pore diameter about 7.4 Å [20]. Further, these valuable features of NaX zeolite make it a promising superior adsorbent for various applications such as removal of radioactive elements and heavy metals, natural gas purification, removal of chemical warfare agents, adsorption of dyes, etc. [21, 22]. Various methods including ion exchange, doping, and impregnation [23–25] have been exerted to enhance the adsorption potential of zeolites. Many studies have been reported on the removal of organic dyes from wastewater using NaX [26], NaX/ZnO [27], TiO_2 /NaX [28], Ni/ TiO_2 /NaX [29], and other materials. In present research, MgO and TiO_2 NPs as the guest molecules were initially fabricated over the NaX zeolite framework. Then, for the first time, the attained NaX/MgO– TiO_2 , as a novel zeolite nanocomposite adsorbent was applied for the adsorption of methyl orange (MO) anionic dye from aqueous solution. To reach the most effective adsorption reactions, several factors such as pH, adsorbent dose, contact time, adsorbent type, initial concentration, and temperature were evaluated and optimized. Further, the kinetic, isotherm, and thermodynamic reactions of MO dye over the NaX/MgO– TiO_2 zeolite nanocomposite adsorbent were also studied. To the best of our knowledge, there has been no study on the fabrication and performance of this nanocomposite utilized for the adsorption of MO in any previous scientific research.

2 Experimental

2.1 Materials

Aluminum hydroxide ($\text{Al}(\text{OH})_3$, 99%), sodium silicate (Na_2SiO_3 , 98%), sodium hydroxide (NaOH, 98%), titanium isopropoxide (TIP, 97%), isopropyl alcohol (IPA, 99%), magnesium(II) nitrate hexahydrate ($\text{Mg}(\text{NO}_3)_2 \cdot 6\text{H}_2\text{O}$,

98%), ammonia solution (25%), ethanol ($\text{C}_2\text{H}_5\text{OH}$, 99%), hydrochloric acid (HCl, 37%), and methyl orange (MO, $\text{C}_{14}\text{H}_{14}\text{N}_3\text{NaO}_3\text{S}$, 98%) organic dye were used as received from Sigma-Aldrich and Merck.

2.2 Instrumentation

The crystalline size and morphology of the as-prepared samples were fully characterized utilizing the field emission scanning electron microscopy associated with energy dispersive X-ray spectroscopy (FESEM-EDX) and X-ray mapping on a MIRA3 TESCAN scanning electron microscope. Also, the topography and morphology of the synthesised samples were investigated by Atomic force microscopy (AFM) (Noncontact mode, Ara-AFM, Iran, model Full plus). The shape, morphology and particle size of the synthesized samples were observed using Transmission electron microscopy (Philips Holland, model CM120). The X-ray diffraction (XRD) patterns were gained by a STOE diffractometer at wavelength of 1.54056 Å (40 mA and 40 kV) with $\text{CuK}\alpha$ radiation recorded at 2° min^{-1} within the 2θ range of 2° – 91° . Further, a Fourier transform infrared (FTIR) spectroscopy (Schimadzu system 160 spectrophotometer) was used to investigate the functional groups and structural properties from 400 to 4000 cm^{-1} on the KBr pellets. An ultrasonic device (Parasonic; 100 W output acoustic power and frequency of 100 Hz) was applied to prepare the samples and to evaluate the adsorption reactions of MO organic dye. Furthermore, a UV–Vis spectrophotometer (Cary 100, Varian Company) within the wavelength range of 200–800 nm was scanned to obtain the absorption spectrum of the MO dye adsorption reactions.

2.3 Synthesis of the MgO NPs

To synthesize the MgO NPs, initially, a specific amount of $\text{Mg}(\text{NO}_3)_2 \cdot 6\text{H}_2\text{O}$ salt (0.1 M) was poured into deionized water (200 mL). Next, the ammonia solution (25%, 0.5 M) was added dropwise to the above solution under vigorous stirring for 25 min until a pH of 10.5 was achieved. During the addition of ammonia solution, the pH of the solution diminished due to the hydrolysis process of the magnesium (II) nitrate salt. Afterwards, the resulting $\text{Mg}(\text{OH})_2$ gel was placed inside a microwave device for 20 min. Then, the gained precipitate was left to cool down to the room temperature, filtered, and washed several times by deionized water to remove the ionic impurities from its surface. Finally, the attained product was dried in an oven at 120°C for 1 h and subsequently calcined at 550°C for 2 h.

2.4 Synthesis of TiO₂ NPs

In a typical synthesis, titanium isopropoxide (TIP, 10 mL) was added into isopropyl alcohol (IPA, 40 mL) and stirred rapidly for 30 min. On the other hand, a suspension of isopropyl alcohol-deionized water (10 mL with v/v, 1/1) was added dropwise into TIP-IPA solution under vigorous stirring and subsequently sonicated for 1 h. Ultimately, the obtained precipitate was left to dry at 110 °C for 3 h and calcined at 450 °C for 4 h.

2.5 Synthesis of NaX Zeolite

To prepare the NaX zeolite through the hydrothermal method, briefly, an appropriate content of Al(OH)₃ (4.2 g) was dispersed into NaOH aqueous solution (8.4 mL, 50% w/v) at 100 °C. The deionized water (8.5 mL) was then added to the prepared suspension. In the next step, NaOH (15.1 g) was added into this solution and subsequently, deionized water (60 mL) was poured into the solution obtained in the previous step and heated at 50 °C (solution A). On the other hand, Na₂SiO₃ (45.2 g) was added into a solution of deionized water (250 mL) and NaOH (15.2 g) (solution B). Afterwards, the two solutions obtained in previous steps (solutions A and B) were mixed vigorously and the resulting suspension was heated in an oven at 70 °C. The obtained zeolite was thoroughly rinsed using deionized water and finally dried at 80 °C [30].

2.6 Synthesis of NaX/MgO–TiO₂ Nanocomposite

To purvey the NaX/MgO–TiO₂ nanocomposite using the ultrasound-assisted dispersion method, the MgO and TiO₂ NPs (0.5 g) were added into deionized water (50 mL) and the obtained solution was sonicated for 1 h. Afterwards, 1 g of as-prepared NaX zeolite was added to the above solution after which this suspension was vigorously stirred for overnight. The resulting white precipitate was dried at 120 °C for 1 h and the obtained nanocomposite was calcined at 450 °C for 2 h.

2.7 Batch Adsorption Investigations

To investigate the adsorption reactions of methyl orange (MO) dye from aqueous solution, initially, a stock solution (500 mg L⁻¹) of MO dye was purveyed through diluting an adequate amount of the solid MO into deionized water. After that, different concentrations of MO solutions within the range of 50–200 mg L⁻¹ were prepared. Next, the values of 0.1, 0.2, 0.3, 0.4, and 0.5 g L⁻¹ of the synthesized NaX/MgO–TiO₂ nanocomposite were added into 30 mL of MO solutions with different concentrations of 50, 75, 100, 150 and 200 mg L⁻¹, respectively. The attained mixtures were

stirred at time intervals of 5, 10, 15, 20, 25, 30 and 35 min at various temperatures of 298, 308 and 318 K, respectively. The supernatant solutions were then centrifuged and separated from the mixture. To evaluate the values of MO adsorbed on the nanocomposite, the remaining MO dye concentrations in the separated solutions were determined via the ultraviolet–visible (UV–Vis) analysis. To study the influence of pH on the adsorption reactions efficiency, the solution pH was adjusted within the range of 2.5–8.5 using NaOH and HCl aqueous (1 mol L⁻¹). Plus, the effects of other adsorbents including NaX, MgO, TiO₂ and MgO–TiO₂ were also investigated on the adsorption efficiency of MO.

3 Results and Discussion

3.1 Characterization of Nanocomposite

Figure 1 exhibits the Field emission scanning electron microscopy (FESEM) of the as-prepared samples including pristine NaX (Fig. 1a), NaX/MgO–TiO₂ (Fig. 1b, c) and pristine MgO–TiO₂ (Fig. 1d). Comparison between the morphologies of pristine NaX and NaX/MgO–TiO₂ illustrated that the crystalline size and morphology of these two samples were kept intact after the synthesis of MgO–TiO₂ on the surface of NaX zeolite. Additionally, the average crystalline size of the MgO–TiO₂ NPs in the as-synthesized nanocomposite proved to have nanometric ranges between 20 and 30 nm. For the evaluation of the width of particle size distribution of NaX/MgO–TiO₂ nanocomposite, the polydispersity index (PDI) was used. The PDI of this nanocomposite was estimated from Fig. 1c using the following Eq. (1):

$$\text{PDI} = \left(\frac{\sigma}{D} \right)^2 \quad (1)$$

where D is the mean diameter of the NPs and the σ is the standard deviation. The PDI of the particles size was found to be 0.4, indicating that this sample is polydisperse [31]. To investigate the elemental composition of the as-prepared NaX/MgO–TiO₂, the energy dispersive X-ray (EDX) analysis was also employed with the attained results depicted in Fig. 1e. Indeed, the obtained results from EDX analysis affirm the presence of four main elements including Na, Al, Si, and O in the pristine NaX and NaX/MgO–TiO₂, which is in good agreement with the acquired data from FESEM analysis. Furthermore, investigating Fig. 1e, the presence of both Mg and Ti elements in the NaX/MgO–TiO₂ can be confirmed. Meanwhile, Fig. 1f reveals the FESEM micrograph related to EDX elemental dot-mappings of the synthesized nanocomposite. From these elemental mappings, the uniform distributions of aforementioned elements and homogeneity of nanocomposite can be verified. Also, the as-prepared samples were well scrutinized through the atomic

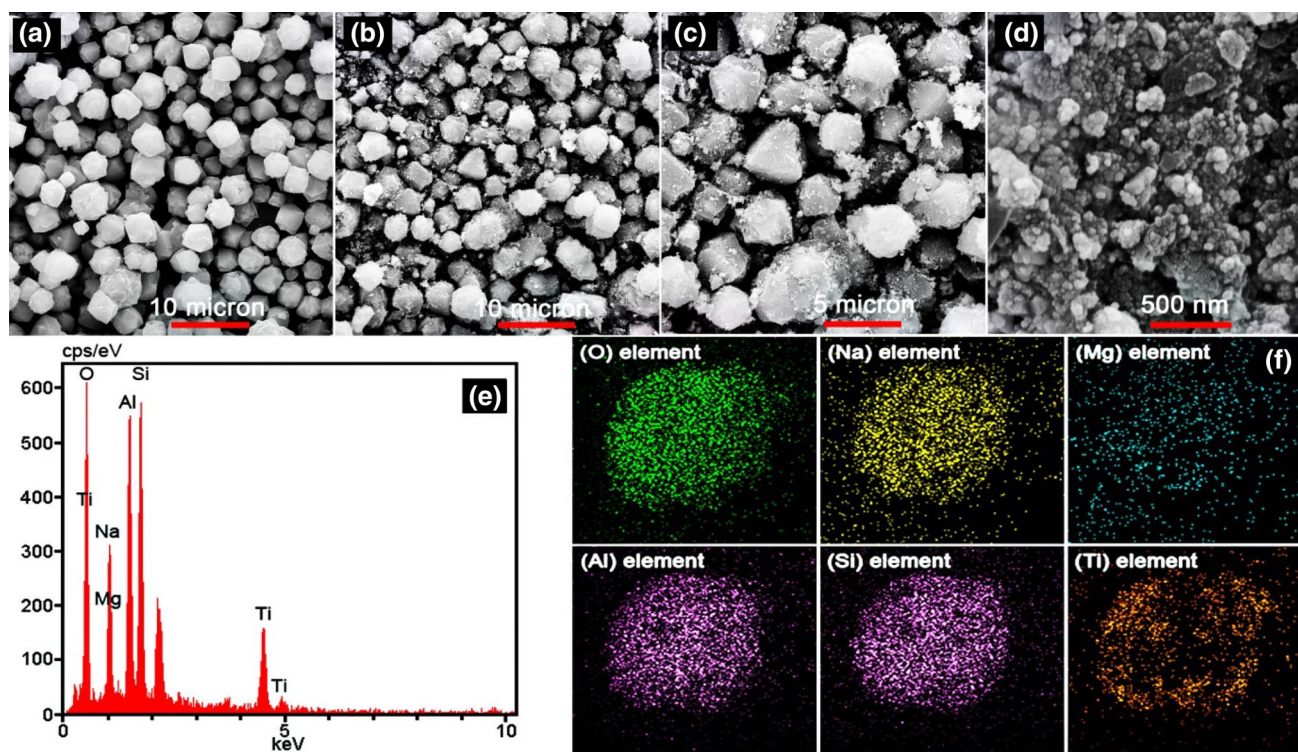


Fig. 1 FESEM micrographs of: **a** pristine NaX, **b, c** NaX/MgO–TiO₂, and **d** pristine MgO–TiO₂. **e** EDAX and **f** EDAX dot-mappings analyses of NaX/MgO–TiO₂

force microscopy (AFM) analysis. The AFM analysis is a valuable method to evaluate different structural properties such as surface topography, roughness, and crystalline size of the adsorbent. The obtained results assigned to the pristine NaX (Fig. 2a, b) and NaX/MgO–TiO₂ (Fig. 2c, d) have been demonstrated in Fig. 2. As can be indicated from Fig. 2c, d, it is deduced that the 2D and 3D AFM micrographs reflect the formation of NaX/MgO–TiO₂ nanocomposite framework. Furthermore, this fact emphasizes that the particle size of the as-prepared NaX/MgO–TiO₂ nanocomposite is in good agreement with the attained structure of the aforementioned nanocomposite from FESEM analysis. The morphology of the prepared samples including pristine NaX (Fig. 3a) and NaX/MgO–TiO₂ nanocomposites (Fig. 3b) were investigated by Transmission electron microscopy (TEM) analysis. As can be seen from TEM micrograph (Fig. 3b), the MgO–TiO₂ nanoparticles were located on the NaX zeolite. According to the TEM micrograph of the NaX/MgO–TiO₂ nanocomposite, the sample consists of MgO–TiO₂ nanoparticles with an average size of about 26 nm that covers the surface of NaX zeolite. These results were consistent with those obtained by AFM and SEM analyses. The X-ray diffraction (XRD) patterns of the pristine NaX (Fig. 4a), NaX/MgO–TiO₂ (Fig. 4b) and pristine MgO–TiO₂ (Fig. 4c) have been depicted in Fig. 4. Base on the diffraction patterns in Fig. 4a, several narrow peaks due

to the NaX zeolite were recognized at 2θ values of 6.90°, 9.90°, 11.69°, 15.406°, 23.29°, 26.64°, and 30.29° attributed to the diffraction planes of (111), (220), (311), (331), (511), (440), and (620), respectively with cubic structure (ICSD card # 41-0118). Moreover, the ten peaks of TiO₂ phase appeared at approximately $2\theta = 25.28^\circ, 37.80^\circ, 48.05^\circ, 53.91^\circ, 55.06^\circ, 63.07^\circ, 69.23^\circ, 70.89^\circ, 75.38^\circ,$ and 33.35° (Fig. 3b), which are referred to the Bragg's reflection planes (101), (004), (200), (105), (211), (204), (116), (220), (215), and (224), respectively with ICSD card # 21-1272. Meanwhile, other clear peaks indicated at $2\theta = 36.38^\circ, 42.14^\circ, 62.57^\circ, 74.05^\circ$ and 78.68° which are assigned to the diffraction planes of (111), (200), (220), (311), and (222) and also related to the MgO NPs with ICSD card # 45-946. No characteristic peaks attributed to the existence of impurities were revealed in the diffraction patterns after the synthesis of MgO–TiO₂ NPs. In addition, by synthesizing the MgO–TiO₂ NPs over the NaX zeolite, the structure of this zeolite did not change and can be stable after the immobilization process. Moreover, the crystalline size of the fabricated MgO–TiO₂ NPs over the NaX zeolite framework was estimated via the XRD analysis utilizing the Debye–Scherrer Equation as follows (2):

$$d = 0.9\lambda / \beta \cos\theta \quad (2)$$

Fig. 2 2D and 3D AFM micrographs of: **a** and **b** pristine NaX, and **c** and **d** NaX/MgO–TiO₂

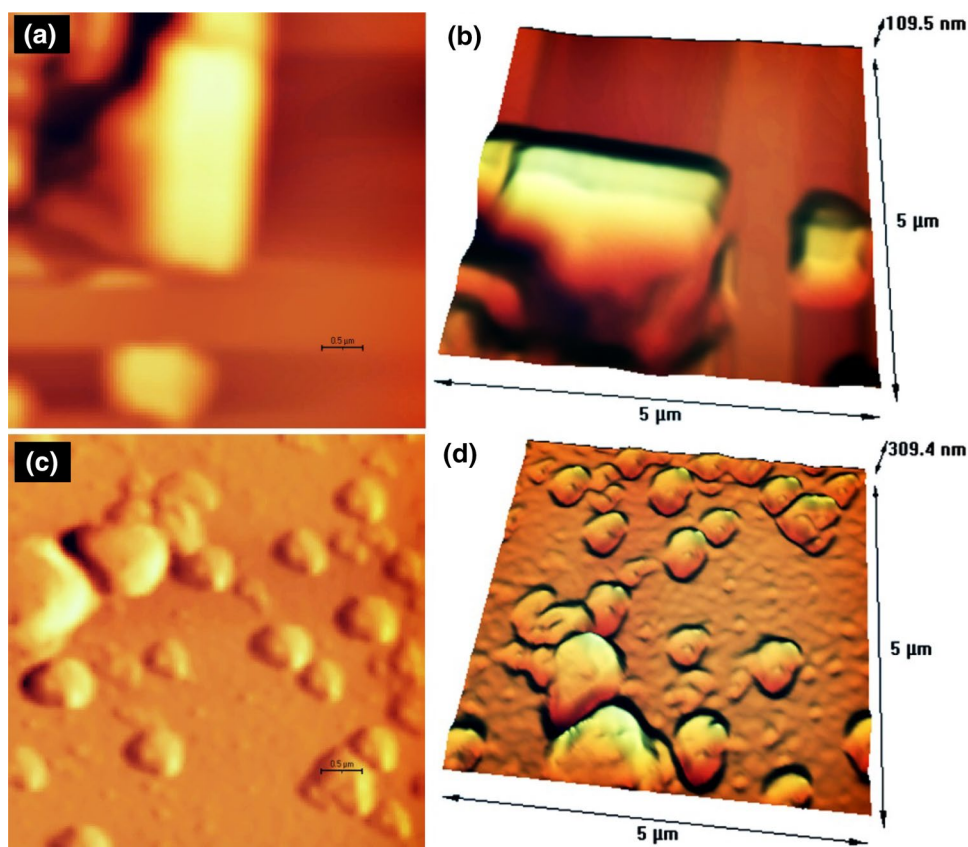
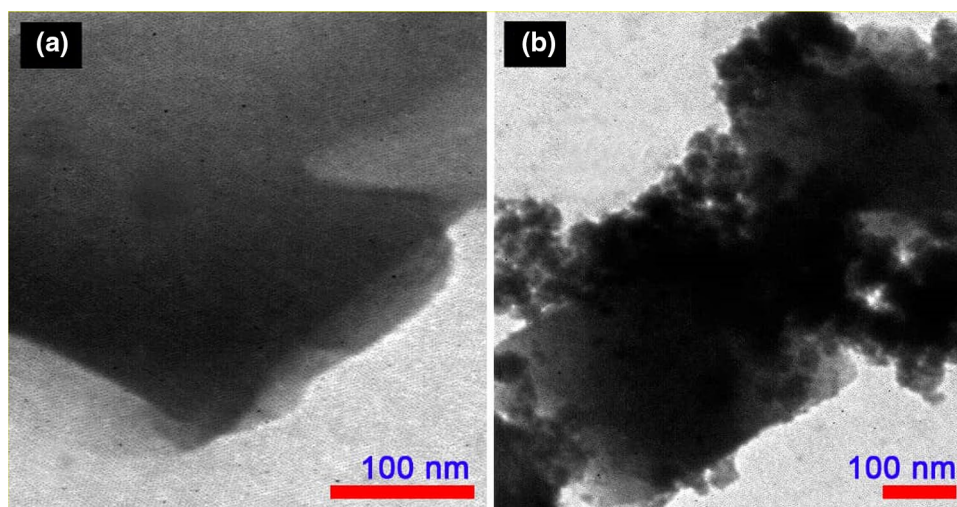


Fig. 3 TEM micrographs of: **a** pristine NaX and **b** NaX/MgO–TiO₂



In the aforementioned equation, the crystalline size is revealed utilizing d parameter, λ is related to the wavelength of CuK α radiation, β is the full width at half maximum (FWHM) and also θ parameter refers to the Bragg diffraction angle. Using the above equation, the average crystalline size was determined approximately 24 nm. It is approved that the estimated average particle sizes from MgO to TiO₂ NPs in the NaX/MgO–TiO₂ nanocomposite are in good agreement with those of AFM and FESEM analyses.

To study the functional groups and structural properties of the synthesized samples, the Fourier transform infrared spectroscopy (FTIR) analysis was applied. The corresponded FTIR spectra of the pristine NaX (Fig. 5a), NaX/MgO–TiO₂ (Fig. 5b) and pristine MgO–TiO₂ (Fig. 5c) have been displayed in Fig. 5. As elucidated from Fig. 5a, b, it is confirmed that the defined peaks positions are nearly the similar for those two types of NaX zeolite. The peaks around 462 cm⁻¹ and 509 cm⁻¹ are corresponded to the the internal

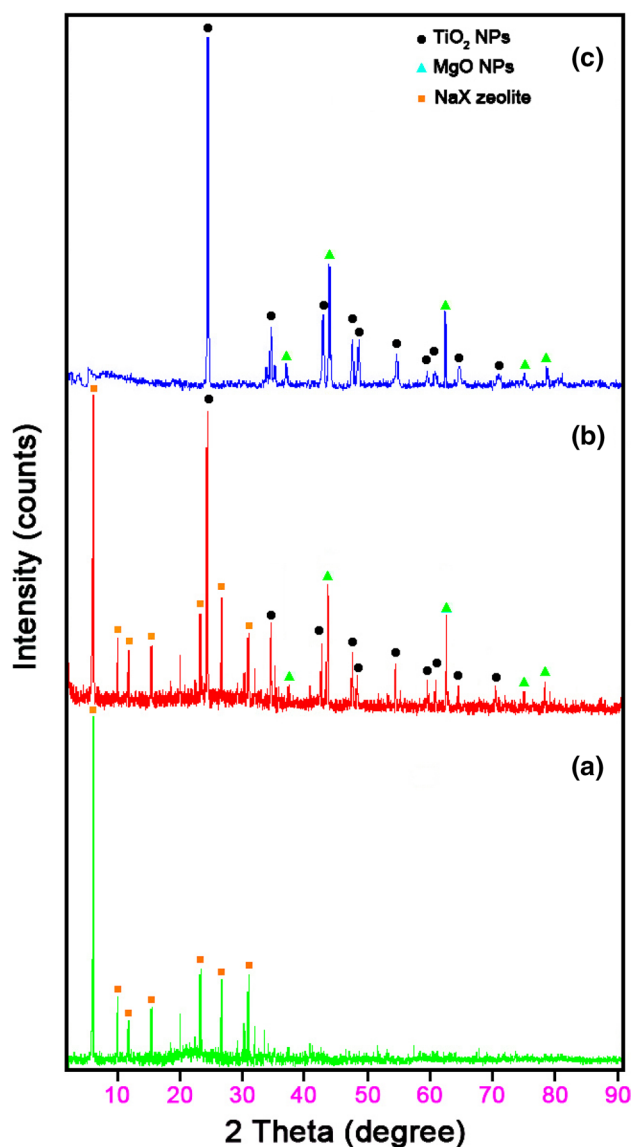


Fig. 4 XRD patterns of: **a** pristine NaX, **b** NaX/MgO-TiO₂ and **c** pristine MgO-TiO₂

SiO₄ or AlO₄ tetrahedral units and bending vibrations of the D6R external linkage of NaX zeolite, respectively. Also, the appeared peaks at 621 cm⁻¹ and 750 cm⁻¹ are due to the external linkage and vibrations O-T-O internal tetrahedral symmetrical stretching, respectively. Furthermore, the peak around 977 cm⁻¹ is affiliated to the O-T-O external connection and internal tetrahedral asymmetrical stretching vibrations of the NaX zeolite. The peaks at 1625 cm⁻¹ and 3406 cm⁻¹ are assigned to the H₂O absorption bonds and vibrations of hydroxyl group in the NaX framework, respectively. Besides, the comparison between Fig. 5a, b revealed no significant change in the structure of NaX zeolite after the synthesis of MgO-TiO₂ NPs over it was observed. On the other hand, The identified bands assigned

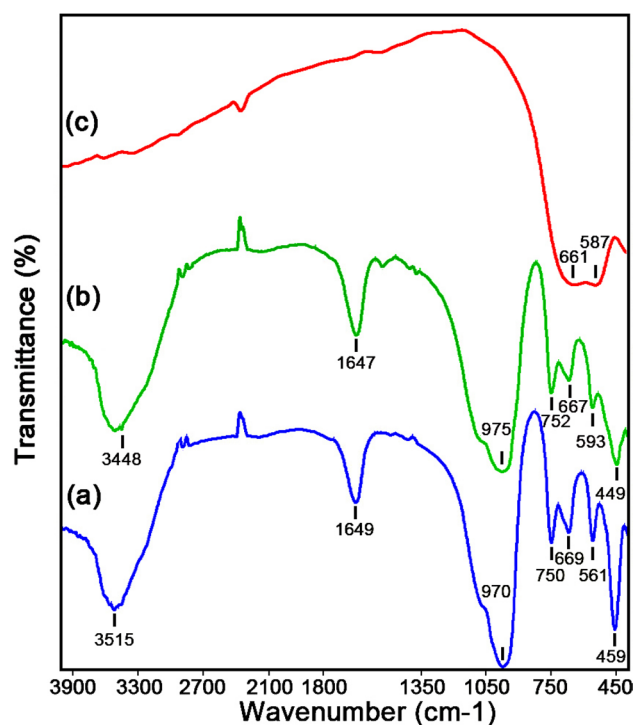


Fig. 5 FTIR spectra of: **a** pristine NaX, **b** NaX/MgO-TiO₂ and **c** pristine MgO-TiO₂

to the Si-O-M and/or Al-O-M of MgO-TiO₂ NPs (M=Mg and/or Ti) expected between 400 and 1000 cm⁻¹, were not precepted owing to the overlapping with the bands affiliated to the NaX. Meanwhile, Fig. 5c shows the FTIR spectrum of the pristine MgO-TiO₂ NPs. The observed peaks between 400 and 700 cm⁻¹ related to the stretching vibrations of Mg-O and Ti-O bonds, respectively.

3.2 Adsorption Evaluation

To a 50 mg L⁻¹ of MO dye solution (optimized value), 0.3 g L⁻¹ of NaX, MgO, TiO₂, MgO-TiO₂ and NaX/MgO-TiO₂ adsorbents were added and stirred rapidly for 35 min at 45 °C. The samples were then separated from supernatant by centrifuging the solution. To determine the amount of adsorbed MO by the adsorbents, MO concentrations were measured before and after the adsorption by UV-Vis technique. In addition, the impacts of several parameters including pH, adsorbent dose, contact time and initial concentration, and also kinetics and thermodynamic reactions were studied.

3.3 Effect of Solution pH

The impact of initial solution pH on the adsorption of MO using the NaX/MgO-TiO₂ nanocomposite is revealed in Fig. 6a. It is observed that for 50 mg L⁻¹ of MO

concentration at 45 °C, the adsorption percentage of methyl orange is dependent on the pH of solution. In this work, the adsorption process of MO was examined within the pH range of 2–9. The highest adsorption percentage for MO was obtained at pH 6.5. The solution pH was adjusted via 1 mol L⁻¹ solutions of sodium hydroxide and hydrochloric acid. Thus, pH=6.5 was chosen as optimized pH for adsorption of MO by the NaX/MgO–TiO₂ nanocomposite.

3.4 Effect of Adsorbent Dose

Determination of optimized dosage of an adsorbent is important factor in the adsorption system by the adsorbent. The idea adsorbent is the one whose minimum concentration offers the highest absorption efficiency. In this work, to find the best and optimized adsorbent dose for the adsorption of MO dye, the adsorption process of MO was investigated within the range of 0.1–0.5 g L⁻¹ of NaX/MgO–TiO₂. As can be seen in Fig. 6b, the adsorption

percentage grew with the rise of the dose of adsorbent, after which no more notable variations occurred. Therefore, the value of 0.3 g L⁻¹ was chosen as the optimized dose for NaX/MgO–TiO₂ to perform high yield adsorption process.

3.5 Effect of Contact Time

In this research, the influence of contact time on the adsorption efficiency of MO over the NaX/MgO–TiO₂ nanocomposite was investigated. Figure 6c displays the variations in the amount of dye adsorbed with shaking time as well as the reliability of adsorption yield of MO on the NaX/MgO–TiO₂ adsorbent over the contact time. The contact time was studied within the range of 0–35 min. The obtained results indicated that adsorption amount of MO increased over the contact time, where the adsorption increased up to 35 min. Therefore, period of time 35 min was selected as optimized time.

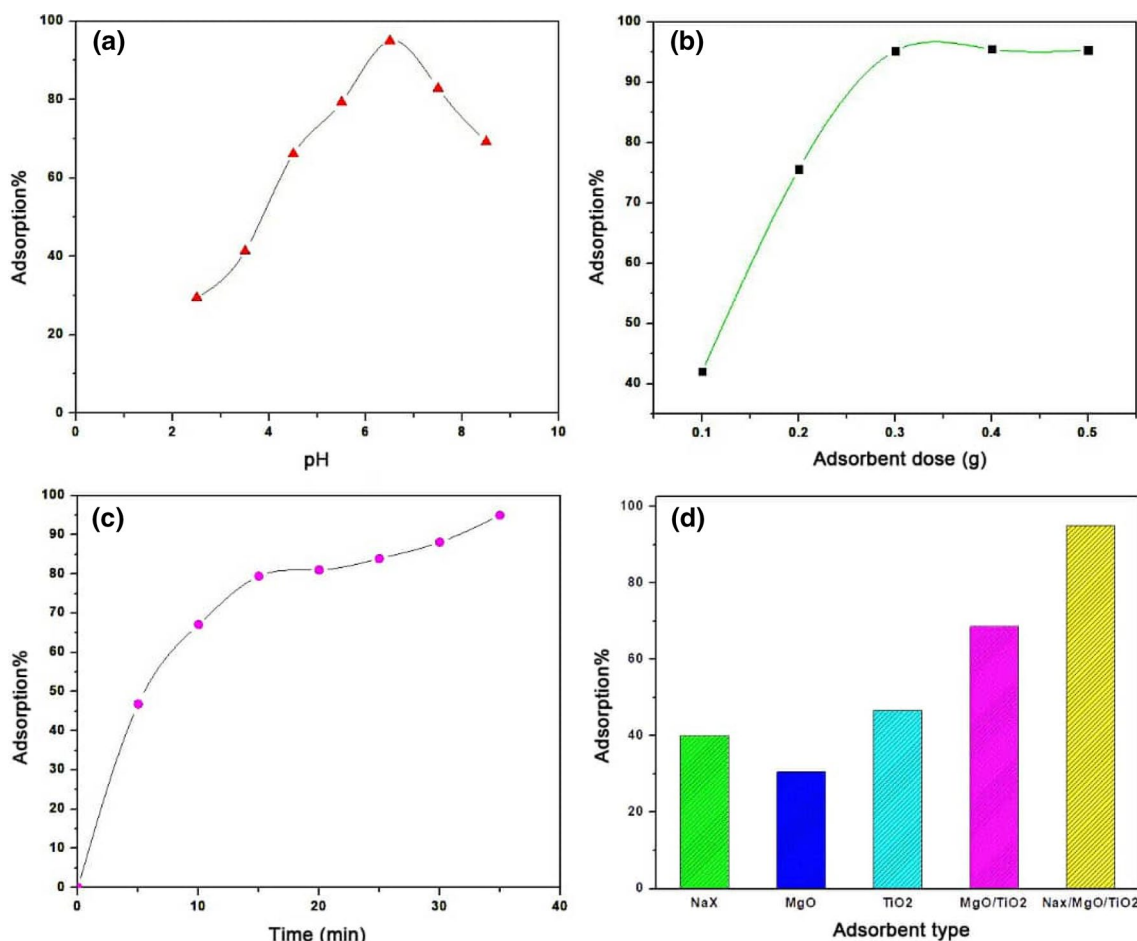


Fig. 6 Effect of solution pH (a), adsorbent dose (b), contact time (c) and adsorbent type (d) on the adsorption efficiency of MO dye over the NaX/MgO–TiO₂ zeolite nanocomposite adsorbent

3.6 Effect of Adsorbent Type

To evaluate the effect of adsorbent type on the adsorption of MO dye, experiments were studied in the presence of different adsorbents including NaX, MgO, TiO₂, MgO–TiO₂ and NaX/MgO–TiO₂. The adsorption efficiencies of MO over the MgO, NaX, TiO₂, MgO–TiO₂ and NaX/MgO–TiO₂ were reached more than 30%, 40%, 46%, 68% and 95%, respectively (Fig. 6d). From the gathered results, it is deduced that the maximum efficiency is related to the NaX/MgO–TiO₂ nanocomposite adsorbent under similar conditions.

3.7 Effect of Initial MO Concentration

Figure 7a–d show the effect of initial MO concentration within the range of 50 to 200 mg L⁻¹ on the adsorption of this dye on the NaX/MgO–TiO₂. It can be seen that

percentage of MO adsorption decreased with the increase in the initial concentration of MO due to the constant amount of adsorbents used in this work. On the other hand, the MO percentage of adsorption was found above 95% for initial concentration of 50 mg L⁻¹, which was 40.6% for that of 200 mg L⁻¹.

3.8 Adsorption Isotherms

In this study, several isotherm models including Langmuir, Freundlich and Temkin models were used for describing the sorption mechanism, affinities of the adsorbent, and the surface properties interaction. These models were studied at pH = 6.5, temperature of 45 °C and different initial solution concentrations (50–200 mg L⁻¹).

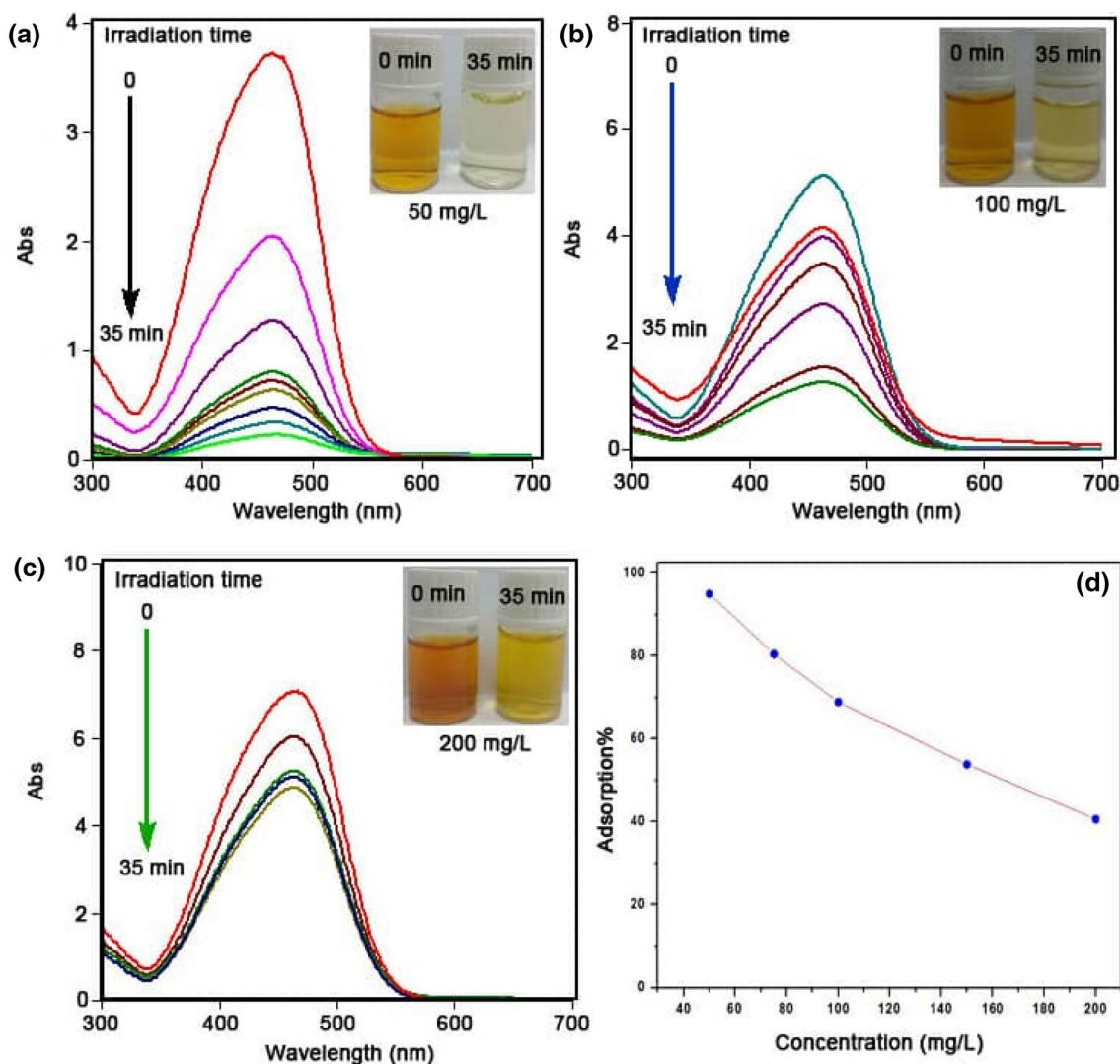


Fig. 7 Effect of initial concentration on the adsorption efficiency of MO dye over the NaX/MgO–TiO₂ zeolite nanocomposite adsorbent (a–d)

3.8.1 Langmuir Isotherm

The Langmuir isotherm is useful in describing the adsorption process of adsorbate on the surface of the adsorbent. This isotherm is most widely applied to a homogeneous adsorption surface with all adsorption sites having equal adsorbate affinity. Thus, Langmuir adsorption isotherm was chosen for estimation of maximum adsorption capacity of the considered adsorbent. The Langmuir isotherm can be expressed via the Eq. (2) [32]:

$$\frac{1}{q_e} = \frac{1}{K_L q_m} \times \frac{1}{C_e} + \frac{1}{q_m} \quad (3)$$

where, q_m , K_L , and C_e are the maximum MO uptake per unit mass of adsorbent, Langmuir constant and the equilibrium concentration of the adsorbent, respectively. The plot of $\frac{1}{q_e}$ versus $\frac{1}{C_e}$ is represented in Fig. 8a.

3.8.2 Freundlich Isotherm

The Freundlich isotherm is an empirical equation commonly used for describing the adsorption process on heterogeneous surfaces. The Freundlich isotherm Equation is expressed as follows (4 and 5) [33]:

$$q_e = K_F C_e^{\frac{1}{n}} \quad (4)$$

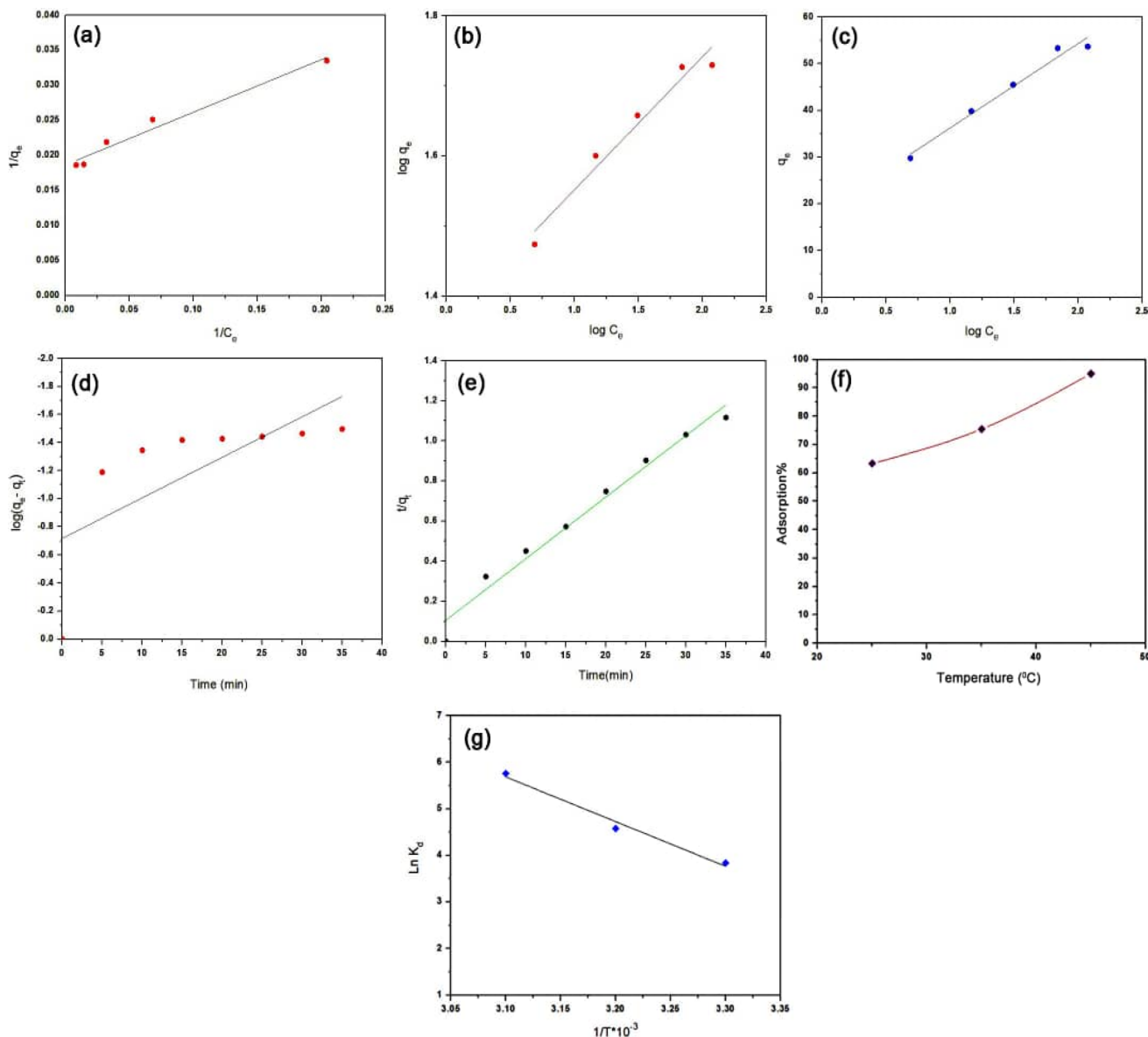


Fig. 8 The Langmuir (a), Freundlich (b) and Temkin (c) isotherm plots, pseudo-first (d) and pseudo-second (e) order kinetics plots, and MO adsorption % versus temperature (f) and the Vans Hoff plot ($\ln K_d$ versus $1/T$) plots (g)

$$\log q_e = \log K_F + \frac{1}{n} \log C_e \quad (5)$$

here, K_F is the constant of Freundlich isotherm [(mg g⁻¹)/(mg L⁻¹)] and n is a factor related to the adsorption tendency determined from the intercept and slope of the plot. The plot $\log q_e$ versus $\log C_e$ is shown in Fig. 8b.

3.8.3 Temkin Isotherm

The linear form of Temkin isotherm is represented through Eq. (6) [34]:

$$q_e = \beta \log \alpha + \beta \log C_e \quad (6)$$

where, α and β are Temkin adsorption constants. This isotherm is usually applied for heterogeneous surface energy systems (non-uniform distribution of sorption heat). The plot of this isotherm which gives a straight line of slope q_e versus $\ln C_e$ is presented in Fig. 8c. The obtained data from these models are summarized in Table 1. According to the R^2 value, high regression correlation coefficient was recognized in appropriate straight linear with the Langmuir ($R^2=0.9822$) isotherm as compared to the Freundlich ($R^2=0.9778$) and Temkin ($R^2=0.9613$) isotherm models.

3.9 Adsorption Kinetics

For the adsorption kinetics study, particularly for measuring the rates of reaction under different experimental conditions, determining the effect of concentration and temperature on reaction rates, specifying the time required for achieving the equilibrium during the adsorption procedure, the kinetic investigations are performed. For adsorption kinetics investigation, the samples were prepared by adding 0.3 g L⁻¹ of NaX/MgO–TiO₂ at pH 6.5 while the MO concentration was 50 mg L⁻¹ in separate containers at 45 °C at certain time intervals. Finally, the samples were collected via membrane filters and afterward tested using ultraviolet–visible (UV–Vis) spectroscopy. The MO adsorption magnitude at time t , q_t (mg g⁻¹), was calculated by the following Eq. (7):

$$q_t = (C_0 - C_e)V/W \quad (7)$$

here, C_0 and C_t are the MO concentrations in the original solution and after time t , respectively. V is the volume

of the solution, and W represents the mass of the NaX/MgO–TiO₂ used. The adsorption kinetics of MO onto the NaX/MgO–TiO₂ adsorbent were measured via pseudo first and pseudo second order models.

3.9.1 Pseudo-First-Order Model

Equation (8) represents Pseudo-first-order model as follows [35]:

$$\log (q_e - q_t) = \log q_e - \frac{k_1}{2.303} t \quad (8)$$

where, q_e and q_t (mg g⁻¹) are the adsorption capacity of MO at equilibrium and at time t , respectively, k_1 is the pseudo-first-order constant (min⁻¹). The values of q_e and k_1 were specified from the intercept and slope of Fig. 8d, respectively. $\log (q_e - q_t)$ was also plotted versus time, where a straight line should be obtained with a slope of k_1 , if the first-order kinetics is credible.

3.9.2 Pseudo-Second-Order Model

The McKay suggested a pseudo-second-order model for the adsorption of MO onto the nanocomposite according to the Eq. (9):

$$\frac{t}{q_t} = \frac{1}{k_2 q_e^2} + \frac{t}{q_e} \quad (9)$$

where, q_e and q_t represent the amounts of MO (g mg⁻¹) at equilibrium and other time intervals. k_2 refers to the rate constant of the pseudo-second-order equation (g mg⁻¹ min⁻¹). When the second-order model is an appropriate expression, a pattern of $\frac{t}{q_t}$ against time (t) will yield a linear result with a slope of $\frac{1}{q_e}$ and an excise of $\frac{1}{k_2 q_e^2}$. The adsorbed amounts (q) of MO were calculated using the Equation below (10) [36]:

$$q = \frac{(C_0 - C_e) \times V}{m} \quad (10)$$

where, C_0 and C_e represent the initial and equilibrium concentrations of MO (g mg⁻¹) in the liquid phase, respectively, V shows the volume of solution (L) and m denotes the mass

Table 1 The adsorption isotherms data for the adsorption of MO over the NaX/MgO–TiO₂ zeolite nanocomposite adsorbent (optimized conditions; initial pH 6.5, adsorbent dose: 0.3 g L⁻¹, contact time: 35 min, and temperature: 45 °C)

Isotherm type	Isotherm parameters		Plot equation
Langmuir	$K_L = 0.24$ (L mg ⁻¹) $q_m = 53.76$ (mg g ⁻¹)	$R^2 = 0.9822$	$y = 0.0751x + 0.0186$
Freundlich	$K_F = 0.13$ (mg g ⁻¹) (L mg ⁻¹) $n = 5.26$	$R^2 = 0.9778$	$y = 0.1898x + 1.3619$
Temkin	$\alpha = -2.17$ (g mg ⁻¹) $\beta = 18.05$ (mol ² KJ ⁻²)	$R^2 = 0.9613$	$y = 18.059x + 18.181$

of adsorbent (g). The pattern among $\log(q_e - q_t)$ versus time t and the pattern of t/q versus time t were employed for capturing the rate constant of pseudo-first-order and pseudo-second-order kinetics of the adsorption and correlation coefficient (R^2). Figure 8e demonstrates the plot of pseudo-first-order kinetic. From Fig. 8d, e, and the data in Table 2, it can be concluded that the pseudo-second-order model is the best fitting model as it offers a higher correlation coefficient ($R^2 = 0.9776$) than pseudo-first-order model does ($R^2 = 0.5251$). Therefore, based on the obtained results, the MO adsorption on the NaX/MgO–TiO₂ follows pseudo-second-order model.

3.10 Adsorption Thermodynamics

In this research, the adsorption of MO over the NaX/MgO–TiO₂ nanocomposite was investigated within the temperature range of 25–45 °C under optimized conditions. The effect of temperature on the adsorption of MO over the nanocomposite adsorbent has been demonstrated in Fig. 8f. According to this figure, the adsorption of MO over the NaX/MgO–TiO₂ increased with elevation the temperature. To study the thermodynamic characteristics, all the solutions were prepared with initial MO concentration of 50 mg L⁻¹ and pH 6.5. Thereafter, 0.3 g L⁻¹ of NaX/MgO–TiO₂ were added to prepared the solutions. The prepared solutions were stirred for 35 min at 298–318°K. Then, the obtained solutions were filtered and analysed using a UV–Vis spectrophotometer. Spontaneity of a sorption process MO on the NaX/MgO–TiO₂ can be determined by the thermodynamic parameters such as enthalpy variations (ΔH°), free energy variations (ΔG°) and entropy variations (ΔS°). These parameters were calculated from the Equations below (11 and 12):

$$\Delta G^\circ = \Delta H^\circ - T\Delta S^\circ \quad (11)$$

$$\Delta G^\circ = -RT\ln K_d \quad (12)$$

Hence, R is the universal gas constant (8.314 J.mol⁻¹.K⁻¹), T and K_d are the absolute temperature in kelvin (°K) and the distribution coefficient, respectively [37]. The negative values ΔG° indicate the spontaneous process of MO adsorption onto the NaX/MgO–TiO₂. According to obtained results, the adsorption of MO over the NaX/MgO–TiO₂ could be attributed to a physicochemical adsorption procedure ($\Delta H^\circ = 79.74$ kJ/mol). Also, the positive values of enthalpy ΔH° indicate the endothermic nature of adsorption processe. The positive values of entropy variations ΔS° reflect that no particular change has taken place in the internal structure during the adsorption of MO onto NaX/MgO–TiO₂. The plot of $\ln K_d$ versus 1/T and the gained data from this plot have been revealed in Fig. 8g and Table 3.

3.11 Comparison of the NaX/MgO–TiO₂ Activity with Other Adsorbents

To investigate the activity of the adsorption process, the gained data for the adsorption of MO dye on the NaX/MgO–TiO₂ adsorbent from aqueous solution have been compared to the several mentioned adsorbents in the literature [38–43] and were tabulated in Table 4. These comparisons were implemented based on the maximum capacity of the adsorption process. As can be revealed in this table, the NaX/MgO–TiO₂ can be introduced as an effective and superior adsorbent for the adsorption of MO dye compared to the other applied adsorbents.

3.12 Stability and Regeneration of NaX/MgO–TiO₂

In this study, the stability and regeneration potential of NaX/MgO–TiO₂ nanocomposite adsorbent were studied. For this purpose, the FTIR analysis was employed to investigate the recovered NaX/MgO–TiO₂ for four cycles (Fig. 9a). The adsorption efficiencies of repeating

Table 2 The kinetic models constants for the adsorption of MO over the NaX/MgO–TiO₂ zeolite nanocomposite adsorbent (optimized conditions; initial pH 6.5, adsorbent dose: 0.3 g L, [MO]₀: 50 mg L⁻¹, and temperature: 45 °C)

Kinetic model type	k_1 (min ⁻¹)	k_2 (g mg ⁻¹ min ⁻¹)	R^2	Plot equation
First-order	0.08	–	0.5251	$y = -0.0356x - 0.6501$
Second-order	–	0.34	0.9776	$y = 0.0307x + 0.1064$

Table 3 Thermodynamic data for the adsorption of MO over the NaX/MgO–TiO₂ zeolite nanocomposite adsorbent (optimized conditions; initial pH 6.5, adsorbent dose: 0.3 g L⁻¹, contact time: 35 min, and [MO]₀: 50 mg L⁻¹)

T (°K)	ΔG° (kJ mol ⁻¹)	ΔS° (J mol ⁻¹ K)	ΔH° (kJ mol ⁻¹)	R^2	Plot equation
298	–24.05	294.46	79.74	0.9822	$y = -9.592x + 35.418$
308	–24.85				
318	–25.65				

Table 4 The NaX/MgO–TiO₂ zeolite nanocomposite adsorbent activity compared to the several reported adsorbents on the MO adsorption from aqueous solution

Adsorbent type	q_m (mg g ⁻¹)	References
Diaminoethanesporopollenin biopolymer	4.40	[37]
γ -Fe ₂ O ₃ /SiO ₂ /CS composite	34.29	[38]
Orange peel	20.50	[39]
Natural zeolite modified with hexamethylenediamine	33.00	[40]
Modified ultrafine coal powder	18.52	[41]
Chitosan	34.83	[42]
NaX/MgO–TiO ₂	53.76	Current work

application of NaX/MgO–TiO₂ are displayed in Fig. 9a. The obtained results confirmed no obvious variation in comparison with the fresh NaX/MgO–TiO₂ adsorbent after fourth cycles. Thus, the aforementioned nanocomposite can be applied as a remarkable adsorbent for the adsorption of MO dye from aqueous solution.

4 Conclusion

In this work, we have successfully synthesized the novel NaX/MgO–TiO₂ zeolite nanocomposite adsorbent with the goal to the adsorption of methyl orange (MO) anionic organic dye from aqueous solution. The as-prepared nanocomposite was characterized in detail using FESEM, EDAX, X-ray dot-mapping, AFM, TEM, XRD, and FTIR techniques and subsequently the adsorption reactions were monitored utilizing ultraviolet–visible (UV–Vis) analysis. Moreover, different parameters including pH, adsorbent dose, the contact time, adsorbent type and initial concentration have been assessed and optimized to attain the maximum adsorption yield of MO dye. Also, adsorption equilibrium isotherms were evaluated using the Langmuir, Freundlich and Temkin models. The adsorption data good obeyed the Langmuir isotherm model. The effective chemical parameters such as pH of 6.5, adsorbent dose of 0.3 g L⁻¹, contact time of 35 min, and temperature of 45 °C were examined as the optimized conditions for subsequent processes. The obtained results displayed that NaX/MgO–TiO₂ nanocomposite leads to maximum adsorption of MO dye from aqueous solution. The experimental kinetic was investigated by the pseudo first and pseudo second orders models. The pseudo second order kinetic model exhibits to the best fitted model for the adsorption reaction of MO dye. Additionally, thermodynamic analysis demonstrated that with increasing the temperature, adsorption efficiency increased. Based on the acquired results of this investigation, the NaX/MgO–TiO₂ nanocomposite reveals promising performance as an effective adsorbent for the adsorption of MO dye from aqueous solution.

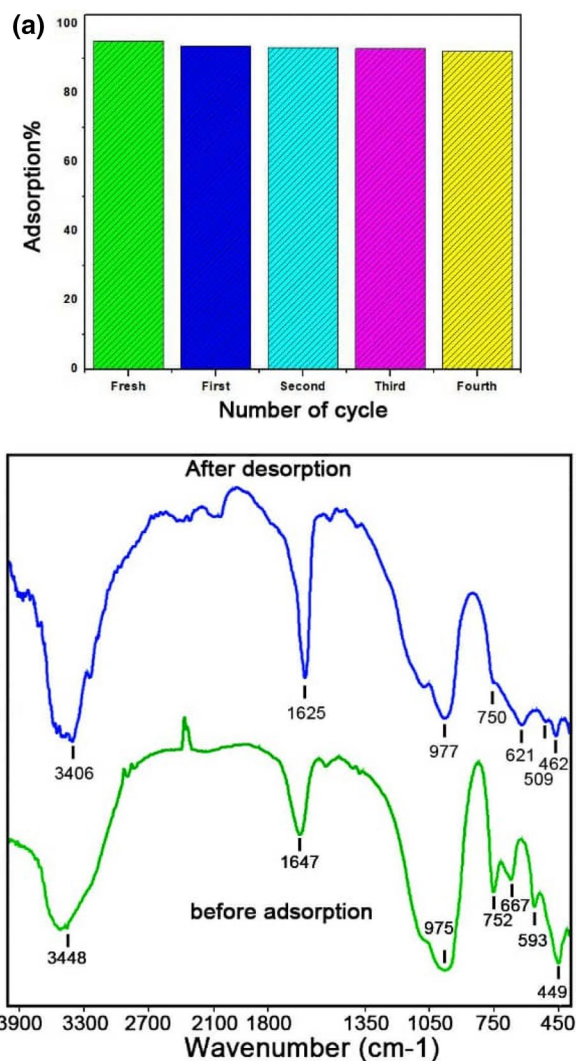


Fig. 9 a Regenerability of NaX/MgO–TiO₂ zeolite nanocomposite adsorbent and b FTIR spectrum of the recovered NaX/MgO–TiO₂ zeolite nanocomposite adsorbent after four cycles in its reaction with MO dye

Acknowledgements The authors give their sincere thanks to the Central lab of Lorestan University, Khorramabad Iran for all supports.

References

- S. Sarmah, A. Kumar, photocatalytic activity polyaniline-TiO₂ nanocomposite. *Indian J. Phys.* **85**, 713–726 (2011)
- A. Mittal, A. Malviya, D. Kaur, J. Mittal, L. Kurup, Studies on the adsorption kinetics and isotherms for the removal and recovery of methyl orange from wastewaters using waste materials. *J. Hazard. Mater.* **148**, 229–240 (2007)
- A. Turki, C. Guillard, F. Dappozze, Z. Ksibi, G. Berhault, H. Kochkar, Phenol photocatalytic degradation over anisotropic TiO₂ nanomaterials: kinetic study, adsorption isotherms and formal mechanisms. *Appl. Catal. B* **163**, 404–414 (2015)
- R. Saraf, C. Shivakumara, S. Behera, H. Nagabhushana, N. Dhananjaya, Facile synthesis of PbWO₄: applications in photoluminescence and photocatalytic degradation of organic dyes under visible light. *Spectrochim. Acta A* **136**, 348–355 (2015)
- Y. Mansourpanah, M. Samimi, Preparation and characterization of a low-pressure efficient polyamide multi-layer membrane for water treatment and dye removal. *J. Ind. Eng. Chem.* **53**, 93–104 (2017)
- N. MuhdJulkapli, S. Bagheri, S. Bee, A. Hamid, Recent advances in heterogeneous photocatalytic decolorization of synthetic dyes. *Sci. World J.* **2014**, 1–25 (2014)
- A. Khataee, R.D.C. Soltani, A. Karimi, S.W. Joo, Sonocatalytic degradation of a textile dye over Gd doped ZnO nanoparticles synthesized through sonochemical process. *Ultrason. Sonochem.* **23**, 219–230 (2015)
- K. Pourzareh, S. Farhadi, Y. Mansourpanah, Anchoring H₃PW₁₂O₄₀ on aminopropylsilanized spinel-type cobalt oxide (Co₃O₄-SiPrNH₂/H₃PW₁₂O₄₀): a novel nanohybrid adsorbent for removing cationic organic dye pollutants from aqueous solutions. *Appl. Organomet. Chem.* **32**, 1–15 (2018)
- M.T. Yagub, T.K. Sen, S. Afroze, H.M. Ang, Dye and its removal from aqueous solution by adsorption: a review. *Adv. Colloid Interface Sci.* **209**, 172–184 (2014)
- S. Rengaraj, A. Banumathi, V. Murugesan, Preparation and characterization of activated carbon from agricultural wastes. *Indian J. Chem. Technol.* **6**, 1–4 (1999)
- A. Metes, D. Kovacevic, D. Vujevic, S. Papic, The role of zeolites in wastewater treatment of printing inks. *Water Res.* **38**, 3373–3381 (2004)
- K.K.H. Choy, G. McKay, J.F. Porter, Sorption of acid dyes from effluents using activated carbon. *Resour. Conserv. Recycl.* **27**, 57–71 (1999)
- Y.-H. Huang, C.-L. Hsueh, C.-P. Huang, L.-C. Su, C.-Y. Chen, Adsorption thermodynamic and kinetic studies of Pb(II) removal from water onto a versatile Al₂O₃-supported iron oxide. *Sep. Purif. Technol.* **55**, 23–29 (2007)
- J. Lee, S. Mahendra, P.J.J. Alvarez, Nanomaterials in the construction industry: a review of their applications and environmental health and safety considerations. *ACS Nano* **4**, 3580–3590 (2010)
- C. Kormann, D.W. Bahnemann, M.R. Hoffmann, Preparation and characterization of quantum size titanium dioxide (TiO₂). *J. Phys. Chem.* **92**, 5196–5201 (1988)
- J. Domaradzki, A. Borkowska, D. Kaczmarek, E.L. Prociow, Properties of transparent oxide thin films prepared by plasma deposition. *Opt. Appl.* **35**, 425–430 (2005)
- J. Zhang, P. Zhou, J. Liu, J. Yu, New understanding of the difference of photocatalytic activity among anatase, rutile and brookite TiO₂. *Phys. Chem. Chem. Phys.* **16**, 20382–20386 (2014)
- T. Somanathan, V.M. Krishna, V. Saravanan, R. Kumar, R. Kumar, MgO nanoparticles for effective uptake and release of doxorubicin drug: pH sensitive controlled drug release. *J. Nanosci. Nanotechnol.* **16**, 9421–9431 (2016)
- C. Mahendirana, K. Scottb, A. Gedankena, Synthesis of a carbon-coated NiO/MgO core/shell nanocomposite as a Pd electrocatalyst support for ethanol oxidation. *Mater. Chem. Phys.* **128**, 341–347 (2011)
- M. Bülow, W. Hilgert, G. Emig, Transport phenomena and reactions in 13X type zeolites, in *Catalysis and Adsorption by Zeolites, Studies in Surface Science and Catalysis*, vol. 65, ed. by G. Öhlmann, H. Pfeifer, R. Fricke (Elsevier, Amsterdam, 1991), pp. 479–490
- D. Akolekar, A. Chaffee, R.F. Howe, The transformation of kaolin to low-silica X zeolite. *Zeolites* **19**, 359–365 (1997)
- M. Murat, A. Amokrane, J.P. Bastide, L. Montanaro, Synthesis of zeolites from thermally activated kaolinite. Some observations on nucleation and growth. *Clay Miner.* **27**, 119–130 (1992)
- M. Sadeghi, S. Yektab, H. Ghaedi, Synthesis and application of Pb-MCM-41/ZnNiO₂ as a novel mesoporous nanocomposite adsorbent for the decontamination of chloroethyl phenyl sulfide (CEPS). *Appl. Surf. Sci.* **400**, 471–480 (2017)
- H. Jahangirian et al., synthesis and characterization of zeolite/Fe₃O₄ nanocomposite by green quick precipitation method. *Dig. J. Nanomater. Bios.* **8**, 1405–1413 (2013)
- T. Yamamoto, E. Apiluck, S. Kim, T. Ohmori, Preparation and Characterization of Cobalt Cation-Exchanged NaX Zeolite as Catalyst for Wastewater Treatment. *J. Ind. Eng. Chem.* **13**, 1142–1148 (2007)
- D. Shakti, B. Sanghamitra, Studies on removal of safranin-T and methyl orange dyes from aqueous solution using NaX zeolite synthesized from fly ash. *Int. J. Sci. Environ. Technol.* **2**, 735–747 (2013)
- F.F. Brites, V.S. Santana, N.R.C. Fernandes-Machado, Effect of support on the photocatalytic degradation of textile effluents using Nb₂O₅ and ZnO: photocatalytic degradation of textile dye. *Top. Catal.* **54**, 264–269 (2011)
- H. Wang, Y. Yu, W. Zhang, Photocatalytic methyl orange degradation on TiO₂-NaX composite. *Adv. Mater. Res.* **129**, 804–809 (2011)
- L. Torkian, E. Amereh, Nano sized Ni/TiO₂@NaX zeolite with enhanced photocatalytic activity. *J. Nanostruct.* **6**, 307–311 (2016)
- M. Rasouli, N. Yaghobi, S. Chitsazan, M.H. Sayyar, Microporous Mesoporous Mater. **90**, 1407–1415 (2012)
- Z. Qin, J. Joo, L. Gu, M.J. Sailor, Size control of porous silicon nanoparticles by electrochemical perforation etching Part. Part. Syst. Charact. **31**, 252–258 (2014)
- I. Langmuir, The adsorption of gases on plane surfaces of glass, mica and platinum. *J. Am. Chem. Soc.* **40**, 1361–1403 (1918)
- E. Voudrias, F. Fytianos, E. Bozani, Sorption Description isotherms of Dyes from aqueous solutions and Waste Waters with Different Sorbent materials. *Global Nest. Int. J.* **4**, 75–83 (2002)
- M.I. Tempkin, V. Pyzhev, Kinetics of ammonia synthesis on promoted iron catalyst. *Acta Phys. Chim. USSR* **12**, 327–356 (1940)
- S. Lagergren, K. Sven, About the theory of so-called adsorption of soluble substances. *Vetenskapsakad. Handl.* **24**, 1–39 (1898)
- Y.S. Ho, G. McKay, The kinetics of sorption of basic dyes from aqueous solution by sphagnum moss peat. *Can. J. Chem. Eng.* **76**, 822–827 (1998)
- R. Niwas, U. Gupta, A.A. Khan, K.G. Varshney, The adsorption of phosphamidon on the surface of styrene supported zirconium (IV) tungstophosphate: a thermodynamic study. *Colloid. Surf. A* **164**, 115–119 (2000)
- M. Küc, A. Kükosmanoglu, O. Gezici, A. Ayar, The adsorption behaviors of methylene blue and methyl orange in a diaminoethane

- sporopollenin-mediated column system. *Sep. Purif. Technol.* **52**, 280–287 (2006)
39. H.Y. Zhu, R. Jiang, L. Xiao, Adsorption of an anionic azo dye by chitosan/kaolin/ γ -Fe₂O₃ composites. *Appl. Clay Sci.* **48**, 522–526 (2010)
40. G. Annadurai, R.-S. Juang, D.-J. Lee, Use of cellulose-based wastes for adsorption of dyes from aqueous solutions. *J. Hazard. Mater.* **92**, 263–274 (2002)
41. E. Alver, A.U. Metin, Anionic dye removal from aqueous solutions using modified zeolite: adsorption kinetics and isotherm studies. *Chem. Eng. J.* **200**, 59–67 (2012)
42. Z. Liu, A. Zhou, G. Wang, X. Zhao, Adsorption behavior of methyl orange onto modified ultrafine coal powder. *Chin. J. Chem. Eng.* **17**, 942–948 (2009)
43. T.K. Saha, N.C. Bhoumik, S. Karmaker, M.G. Ahmed, H. Ichikawa, Y. Fukumori, Adsorption of methyl orange onto chitosan from aqueous solution. *J. Water Resour. Prot.* **2**, 898–906 (2010)

Publisher's Note Springer Nature remains neutral with regard to jurisdictional claims in published maps and institutional affiliations.